Eom *et al. Int J Concr Struct Mater* (2018) 12:76
https://doi.org/10.1186/s40069-018-0312-1

International Journal of Concrete Structures and Materials

RESEARCH Open Access

Time-Dependent Deformations of Eccentrically Loaded Reinforced Concrete Columns

Tae-Sung Eom[1], Chang-Soo Kim[2], Xin Zhang[2] and Jae-Yo Kim[3*]

Abstract

If reinforced concrete columns and walls in high-rise buildings are subjected to axial load for a sustained duration, long-term lateral deformation (or curvature) as well as axial shortening increase over time due to the creep and shrinkage of concrete. In the present study, sustained load tests were performed to evaluate the time-dependent axial shortening and lateral displacement occurring in eccentrically loaded columns. A test set-up using post-tensioning steel rods was introduced for the sustained loading with or without eccentricity. The test results showed that the lateral displacement as well as the axial shortening increased over the sustained duration but the increasing rate of the long-term deformations rapidly decreased with increasing time. The time-dependent axial shortening and lateral displacement increasing with time were predicted by using the age-adjusted effective modulus method based on the creep and shrinkage models of ACI 209. The predictions agreed well with the test results.

Keywords: long-term deformation, sustained load, eccentric loading, long-term curvature, high-rise building, columns, reinforced concrete

1 Introduction

When reinforced concrete (RC) compression members in high-rise buildings are subjected to sustained loads, the creep and shrinkage of concrete increasing with time affect the structural behavior of the members and structures by redistributing stresses between concrete and longitudinal reinforcement. Therefore, current design codes such as ACI 318-14 (ACI Committee 318 2014), KCI (2012), and Eurocode 2 (European Committee for Standardization 2004) recommend that such concrete creep and shrinkage deformations be addressed in the analysis and design of the members and structures particularly in concrete high-rise buildings. As shown in Fig. 1, the columns and walls in irregular high-rise buildings are frequently subjected to bending moment as well as axial load. In such eccentrically loaded columns and walls, lateral displacement (or curvature) as well as axial shortening increase with time due to the creep and shrinkage of concrete. Such long-term lateral displacement can shortly influence differential shortening in buildings under construction and ultimately increase the second-order effects of columns and deflections in beams and slabs. For instance, the differential shortening occurring in compression members such as columns and walls may change initial positions of the beams, slabs, columns, walls, etc. under construction and consequently partitions, architectural finishes, and load transfer between adjacent structural elements are affected (Fintel et al. 1987; Kim and Abdelrazaq 2009; Maru et al. 2003). The moment demand on the columns and walls may be amplified further due to the second-order effects increased by the long-term curvature.

For eccentrically loaded concrete columns, stress redistribution between concrete and reinforcement occurring over time due to sustained loading is more complicated than that in pure compression members. Previous studies were carried out to investigate the time-dependent

*Correspondence: kimjyo@kw.ac.kr
[3] Dept. of Architectural Engineering, Kwangwoon University, 20 Kwangwoon-ro, Nowon-Gu, Seoul 01897, South Korea
Full list of author information is available at the end of the article
Journal information: ISSN 1976-0485 / eISSN 2234-1315

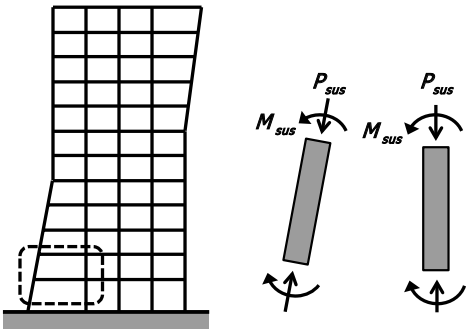

Fig. 1 Columns subjected to bending moment as well as axial compression.

behavior of such eccentrically loaded columns (Viest et al. 1955; Green and Breen 1969; Balaguru and Nawy 1982; Tatsa 1989; Mickleborough and Gilbert 1991; Bradford 1997). Viest et al. (1955) investigated the sustained load-carrying capacity of eccentrically loaded short columns under very high axial compressive load. From the sustained load tests of pin-ended columns without restraints, Green and Breen (1969) reported that the bending moments and curvatures increased with time. Balaguru and Nawy (1982) proposed an analysis method for eccentrically loaded columns based on the creep model of plain concrete. Tatsa (1989) proposed a numerical method for time-dependent analysis, based on the sustained tests on eccentrically loaded panels. Mickleborough and Gilbert (1991) investigated the creep instability of eccentrically loaded slender columns. Bradford (1997) theoretically investigated the flexural rigidity of eccentrically loaded columns under sustained loading.

In the present study, sustained load tests of eccentrically loaded reinforced concrete columns were performed to investigate deformations due to sustained eccentric moment. The test parameters were the magnitude of sustained loads and the presence of eccentricity. The lateral displacement (curvature) and axial shortening due to the sustained eccentric moment were measured through the tests, and the results were compared with the predictions. In addition, simplified methods for estimating the time-dependent deformations of eccentrically loaded columns were proposed, based on the creep and shrinkage models of ACI 209R-92 and the age-adjusted effective modulus method.

2 Test Program

Figure 2a, b show the configurations and reinforcement details of the column specimens. The column specimens were the cantilever with a height of 1460 mm including the pedestal: the heights of the column and pedestal were 1010 mm and 450 mm, respectively. Dimensions of the column and pedestal were 200 mm × 300 mm and 900 mm × 900 mm, respectively. As shown in Fig. 2b, six D16 bars were used as longitudinal reinforcement in the column. All longitudinal reinforcing bars were weld-connected to a 60 mm-thick bearing end plate at the top and were anchored in the pedestal with 90 degree anchorage hook. Tie hoops of D10 bars were placed with a spacing of 100 mm. The first tie hoop was placed at a height of 50 mm from the column base.

Table 1 shows the test parameters. The magnitude of sustained load (P_{sus}) and the presence of eccentricity (e) were considered as the test parameters. Concentrically and eccentrically loaded column specimens were named as C-*xx* and E-*xx*-*y*, respectively. *xx* (=15 and 30) denotes the magnitude of sustained load, P_{sus}, applied to each specimen and y (=1, 2, and 3) denotes the sequential number used for the eccentrically loaded column specimens. C-15 and E-15 were subjected to P_{sus} = 421 kN (=0.15 $A_g f_c'$) and C-30, E-30-1, E-30-2, and E-30-3 were subjected to P_{sus} = 842 kN (=0.30 $A_g f_c'$). A_g = cross section area of column (=60,000 mm^2), and f_c' = concrete strength at 28 days (=47.3 MPa). For the eccentrically loaded column specimens E-15, E-30-1, E-30-2, and E-30-3, the sustained loads P_{sus} were applied with an eccentricity of e = 50 mm from the geometrical center of the cross section. Therefore, in addition to P_{sus}, E-15, E-30-1, E-30-2, and E-30-3 were subjected to the sustained bending moment $M_{sus} = P_{sus}\ e$. As shown in Fig. 2b, the sustained moment M_{sus} was uniform along the column height. The magnitude of the eccentricity was carefully taken as e = 50 mm from a section analysis for short-term loading of P_{sus} and M_{sus} so that the neutral axis lies at the edge of the cross-section (i.e., no tensile stress and no cracking). Note that E-30-1, E-30-2, and E-30-3 were tested under the same sustained load condition in order to improve the reliability of long-term measurement.

Figure 2a shows the test set-up for sustained loading. The compression load P_{sus} was applied by using two external post-tensioning high-strength steel rods (diameter = 38 mm) and a steel block placed on top of the column. At the bottom, the post-tensioning steel rods were pin-jointed to the steel blocks embedded in the concrete pedestal. Twelve shear studs (diameter = 19 mm and extension = 125 mm) were used in each embedded steel block to transfer the post-tensioning loads of the steel rods to the concrete of the pedestal (see Fig. 2a). In order to exclude the contribution of the steel rods to the lateral stiffness of the column, the steel rods were pin-jointed at a height of 90 mm from the column base.

To prevent concrete spalling due to high compressive stress, a steel cap consisting of 60 mm-thick bearing plate and 10 mm-thick side plates was used at the top of the column specimens. (see Fig. 2). In order to

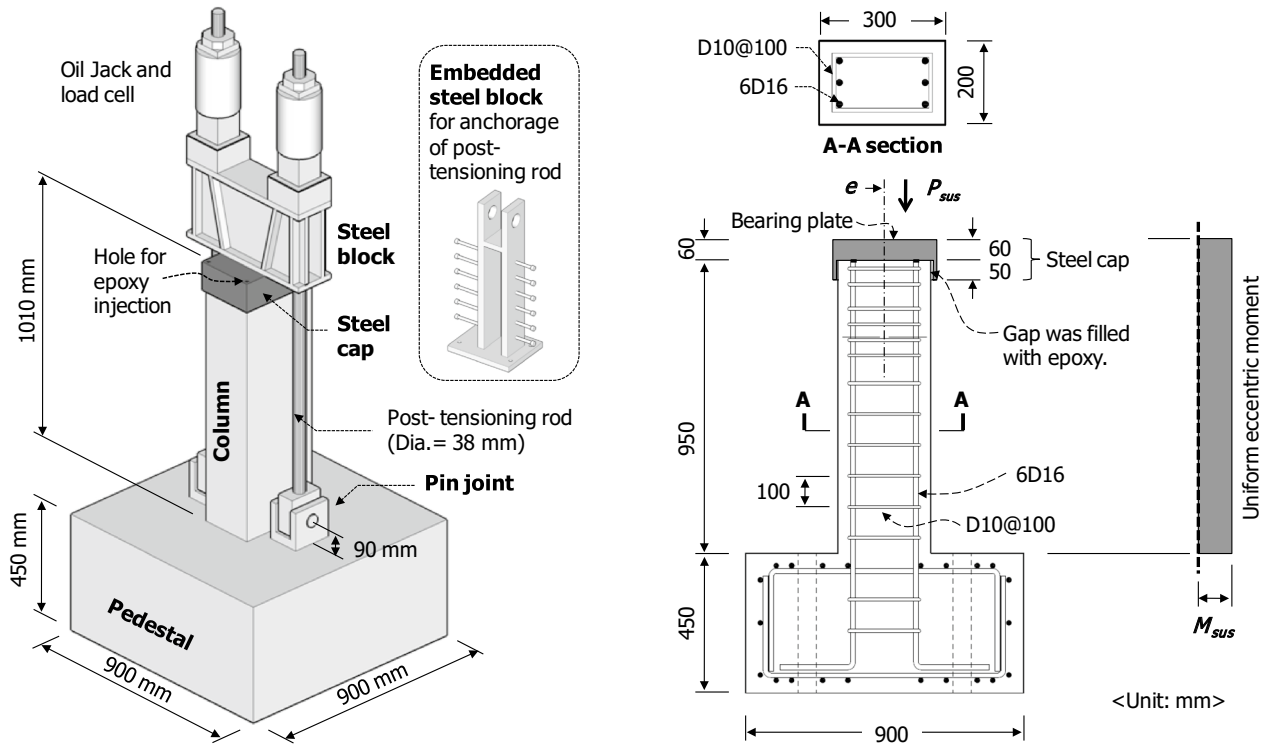

Fig. 2 Configurations and reinforcement details of column specimens.

Table 1 Test parameters of column specimens.

Specimen	Sustained axial load P_{sus} (kN)	Eccentricity e (mm)	Duration (days)
C-15	421	0	64
C-30	842	0	64
E-15	421	50	64
E-30-1	842	50	64
E-30-2	842	50	64
E-30-3	842	50	64

let shrinkage deformation of the concrete occur without restraint during curing, the steel cap was not installed for 2 days before the sustained loading. After the steel cap was placed, the gap between the steel cap and the concrete surface of the columns was filled with high-strength epoxy mortar (see Fig. 2). The epoxy mortar was hardened for 2 days.

Figure 3 shows the strain gages used to measure the long-term strains of the concrete and reinforcing bars during the sustained load tests. The strain gages were placed at three heights, i.e. 100, 400, and 700 mm high from the column base. At each height, four steel and four concrete uniaxial strain gages were used (refer to the section view of Fig. 3). The steel strain gages attached to the reinforcing bars inside concrete while the concrete strain gages were attached to the concrete surface. For eccentrically loaded column specimens, lateral displacement would occur at the top of the columns due to the eccentric moment M_{sus} and continuously increase with time due to the creep and shrinkage of concrete. Therefore, LVDTs were placed at the height of 900 mm from the column base to measure the long-term lateral displacement (see Fig. 3).

3 Sustained Load Test

3.1 Testing Method

The sustained load tests had been performed for 64 days after the initial loading. During the tests, the time-dependent increase in the axial shortening and lateral displacement of the eccentrically loaded columns due to the creep and shrinkage of concrete were measured. Figure 4 shows a photograph of the column specimens placed in the basement laboratory. The sustained loads were applied at the age of 37 days after

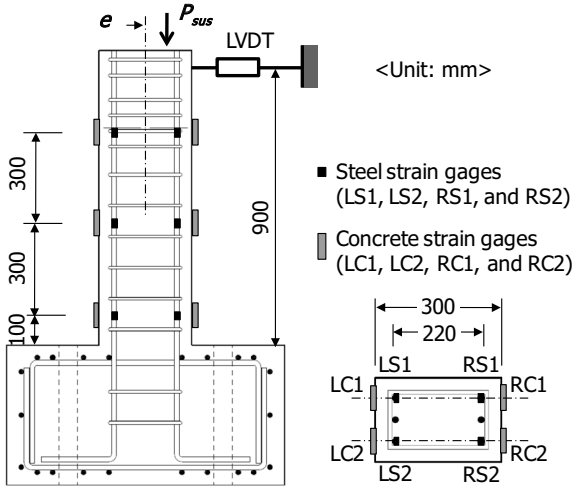

Fig. 3 Measurement of long-term deformations during sustained load tests.

Fig. 4 Sustained load tests.

concrete placement (i.e. $t_0 = 37$ days). The tests were carried out during winter season in Korea. As shown in Fig. 4, the column specimens were placed in the basement laboratory where the variation of temperature and relative humidity between day and night was relatively insignificant. The average temperature and relative humidity of the basement laboratory during the sustained load tests were approximately 8 degrees Celsius and 40%, respectively.

As shown in Fig. 2a, the sustained axial loads were applied by using external post-tensioning high-strength steel rods. The post-tensioning steel rods were stressed by using the oil jacks at the top. Once the target post-tensioning force ($=0.5P_{sus}$) was attained by the oil jacks, the steel nuts were tightened in order for the post-tensioning steel rods to be in place by without loss of the posttensioning force. For precise post-tensioning, the post-tensioning force acting on the steel rods was measured with the load cells. The loss of the post-tensioning force of the steel rods during the sustained load tests were monitored using the strain gages attached to the steel rods.

3.2 Results of Sustained Load Tests

Figures 5 and 6 show the time-dependent deformations of the concentrically and eccentrically loaded column specimens C-30 and E-30-1, respectively. The deformations were measured for the sustained duration of 64 days. In each figure, (a) is the strains of the post-tensioning steel rods, ε_{PT}; (b) is the lateral displacements measured at the top of the column specimens by LVDTs, δ_{LVDT}; (c) and (d) are the compressive strains of the right and left reinforcing steel bars, ε_{RS} and ε_{LS}, respectively; and (e) and (f) are the compressive strains at the right and left concrete faces, ε_{RC} and ε_{LC}, respectively. The measured strains of the post-tensioning steel rods, reinforcing steel bars, and concrete surface, ε_{PT}, ε_{RS}, ε_{LS}, ε_{RC}, and ε_{LC}, are the mean of two measured strains. In Figs. 5c–f and 6c–f, the blue, red, and green lines indicate the strains of the reinforcing bars and concrete at 100, 400, and 700 mm heights from the column base, respectively. As shown in Figs. 5a and 6a, the strains of the posttensioning steel rods decreased over time due to loss of the post-tensioning force. Therefore, when 6, 13, and 41 days passed after the initial posttensioning (i.e. $t - t_0 = 6$, 13, and 41 days), the post-tensioning force of the steel rods were restored to the target force by re-tightening the steel nut using a hand wrench. During the re-tightening process, the measurements of the LVDTs at the top of the columns were disturbed due to the impact of the wrench (see Figs. 5b and 6b). The measurements of the strain gages attached to reinforcing bars and concrete surface were also disturbed during the re-tightening process of the post-tensioning loads (see Figs. 5c–f and 6c–f).

Figures 5 and 6 clearly show the difference in the time-dependent deformations between the concentrically and eccentrically loaded column specimens. As shown in Figs. 5c–f, for concentrically loaded column specimen C-30, the compressive strains of the reinforcing bars and concrete measured at the left and right ends of the cross section were almost identical. Furthermore, the compressive strains increased with time due to creep and shrinkage of the concrete. However, as shown in Fig. 5b, the lateral displacement measured by the LVDT at the top did not increase during the sustained duration. Although sudden changes in the lateral displacement were detected by the LVDT during the re-tightening process,

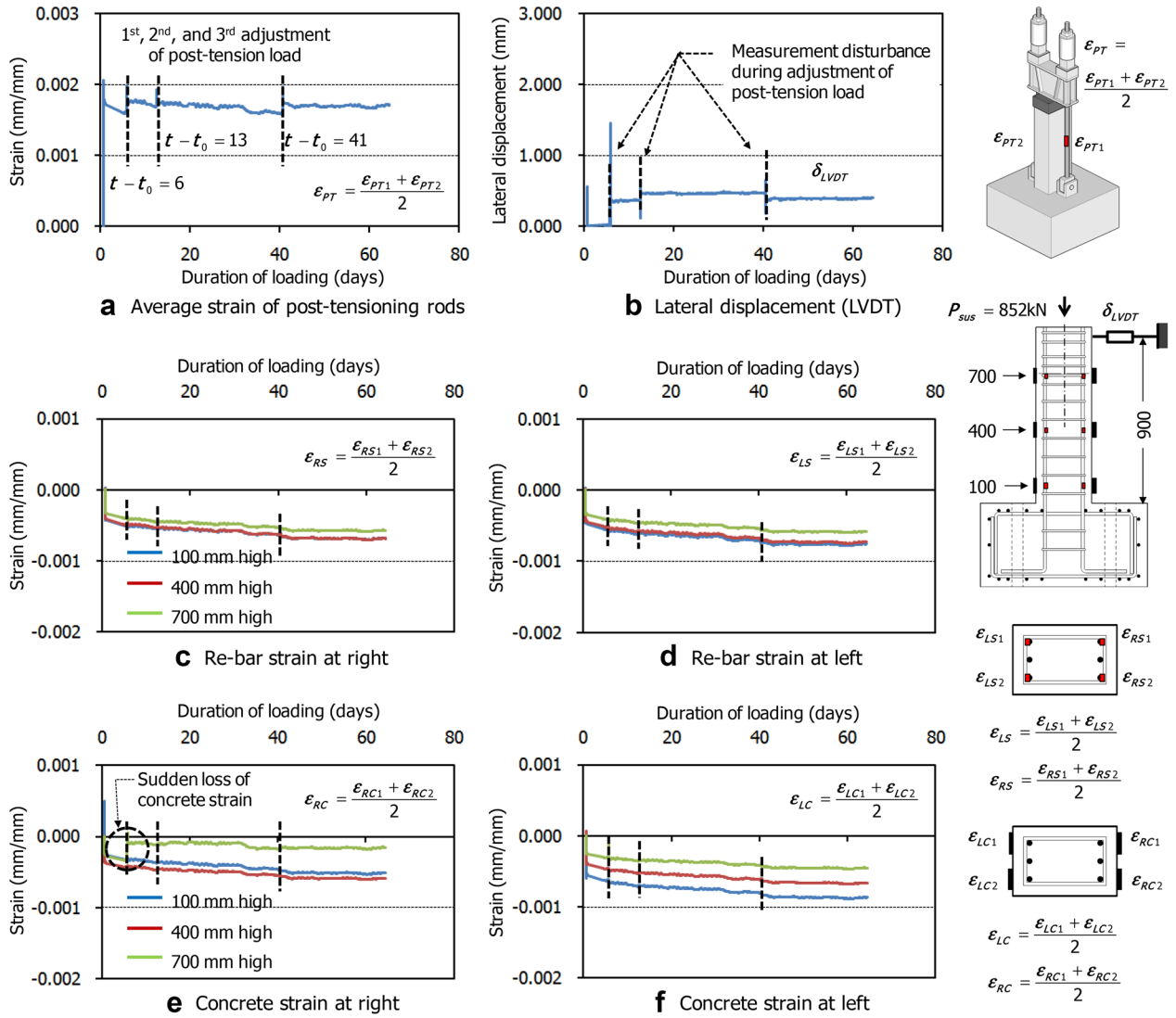

Fig. 5 Long-term measurements of concentrically loaded column specimen C-30.

substantial increase in the lateral displacement with time was not observed.

For eccentrically loaded column specimen E-30-1, however, the lateral displacement occurred on applying the axial load (see Fig. 6b). Furthermore, as shown in Fig. 6c–f, the strains of concrete and reinforcing bars were different at the right and left ends of the cross section. The compressive strains of concrete and reinforcing bars continuously increased with time, but the increasing rates differed. The compressive strains of concrete and reinforcing bars measured at three different heights were nearly identical, which indicates that E-30-1 with an aspect ratio 3.0 (i.e. the ratio of the shear span-to-overall section depth) was subjected to uniform bending moment M_{sus} over the height (compare blue, red, and green lines in Fig. 6c–f).

3.3 Creep and Shrinkage of Concrete Cylinders

Figure 7 shows the developments of creep and shrinkage in the concrete ($f_c' = 47.3$ MPa) with time. For the creep and shrinkage tests, six concrete cylinders with a diameter 150 mm and a height 300 mm were cured inside a water tank for 28 days, and then mounted on the test devices for 90 days. Three concrete cylinders were subjected to compressive stress 14.2 MPa ($= 0.3 f_c'$) for 90 days but the other three were free from compressive stress. The former three concrete cylinders experienced both creep and shrinkage deformations

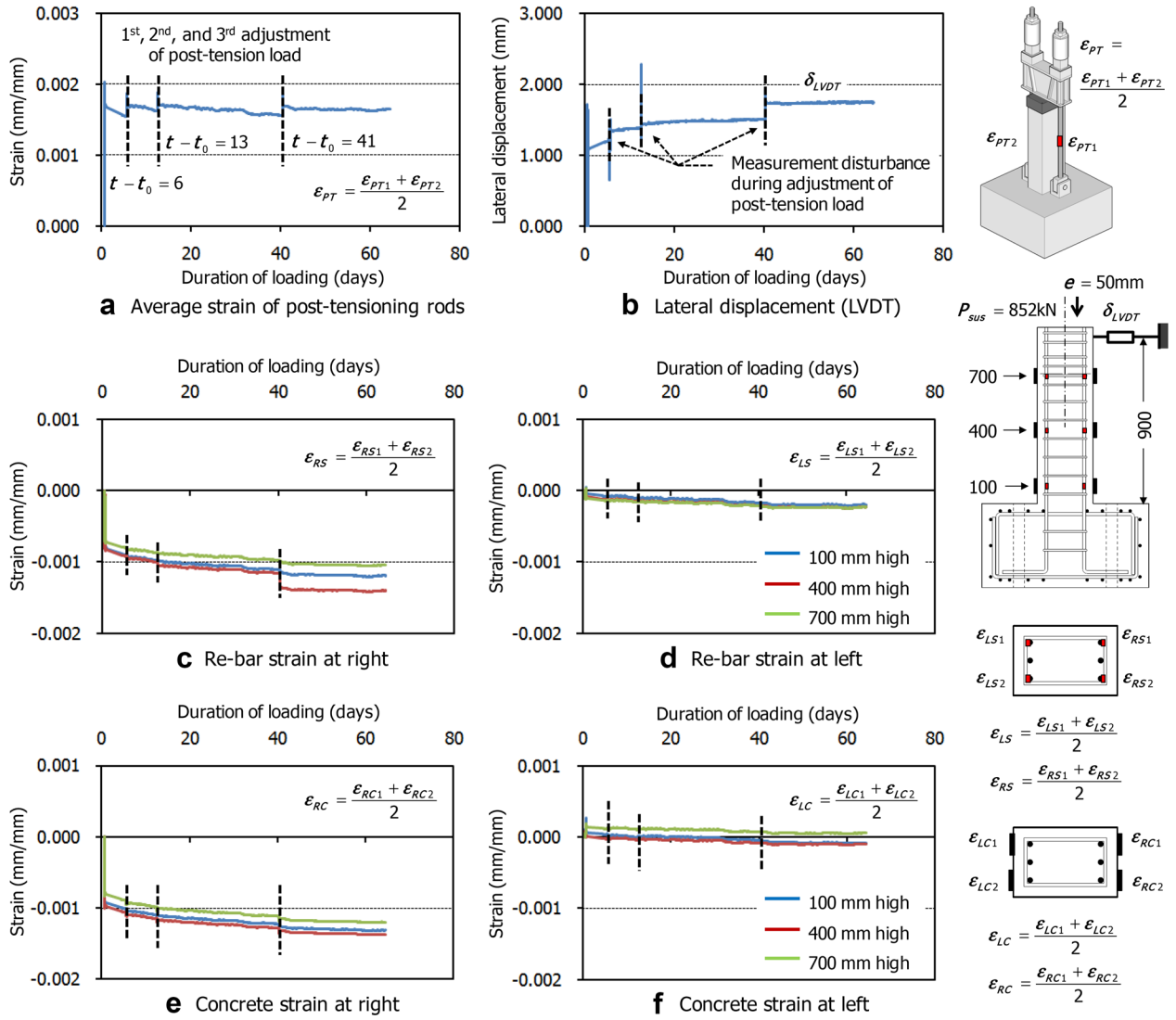

Fig. 6 Long-term measurements of eccentrically loaded column specimen E-30-1.

over time while the latter three concrete cylinders were subjected only to shrinkage. By comparing the time-dependent strains measured from the two groups of concrete cylinders, the creep and shrinkage characteristics of the concrete were evaluated. The room temperature and relative humidity were kept constant with 22.5 °C and 45.3%, respectively.

Figure 7a, b show the creep and shrinkage strains measured for 90 days. The creep and shrinkage strains of one concrete cylinder were significantly deviated from those of the other two concrete cylinders. Therefore, only the results measured from the latter two cylinders were used for the investigation. From a regression analysis, the ultimate creep coefficient and ultimate shrinkage strain of the plain concrete corresponding to the standard conditions of ACI 209R-92 (ACI Committee 209 1992) were determined as $\phi'_u = 2.25$ and $\varepsilon'_{shu} = 0.000672$, respectively. Note that ϕ'_u and ε'_{shu} are the modified values corresponding to the loading age of 7 days and the relative humidity of 40%, though the actual loading age and relative humidity during the tests were 28 days and 45.3%, respectively.

4 Evaluation of Time-Dependent Deformations

Long-term deformations occurring in eccentrically loaded reinforced concrete columns can be evaluated in terms of the axial shortening due to sustained axial compression P_{sus} and the lateral displacement (or curvature)

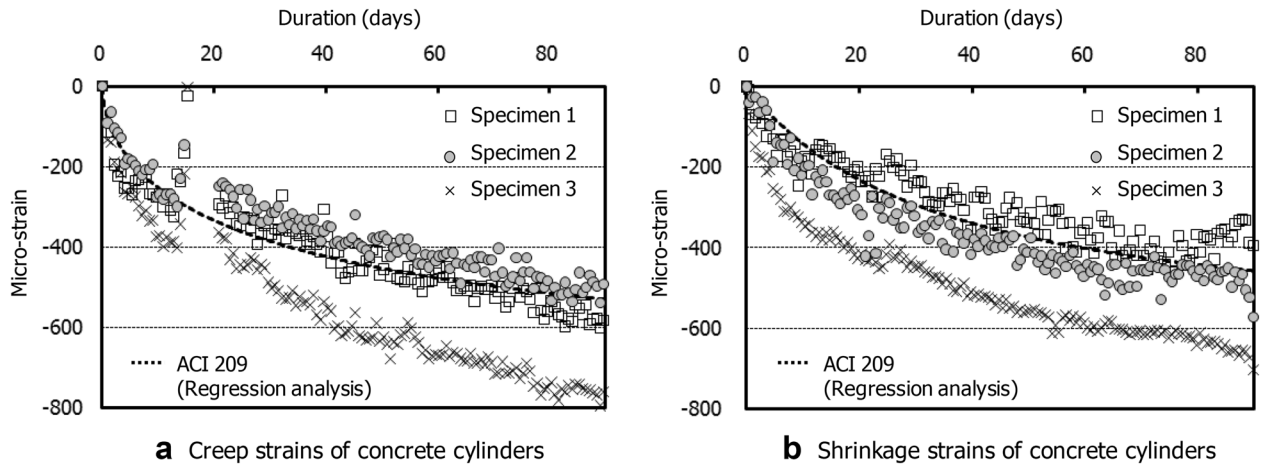

Fig. 7 Creep and shrinkage tests of concrete.

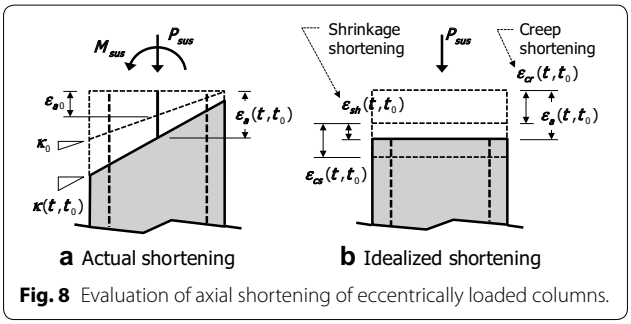

Fig. 8 Evaluation of axial shortening of eccentrically loaded columns.

due to sustained eccentric moment M_{sus}. The eccentrically loaded column specimens of the present study were subjected to compressive stress and strain over the entire cross section without significantly tensile cracking (refer to Fig. 6c–f). Therefore, the long-term axial shortening and curvature were evaluated based on an un-cracked section analysis.

4.1 Axial Shortening

Figure 8a shows the strain distribution at the column section caused by combined axial compression P_{sus} and eccentric moment M_{sus}. The strain distributions due to the immediate loading (i.e. $t = t_0$) and long-term loading are presented as the dotted and thick solid lines, respectively. If the immediate and long-term strain distributions are assumed as linear over the section, the axial shortening strain of eccentrically loaded column can be represented as the strain at the geometrical center of the section (i.e. ε_a and ε_{a0} of Fig. 8a). Furthermore, since the compressive stress–strain relationship of concrete can be approximated as a linear elastic behavior if the compressive stress is not greater than 0.4 f'_c (European Committee for Standardization 2004), the axial shortening of eccentrically loaded column is the same as that of concentrically loaded column (see Fig. 8b).

When reinforced concrete columns are subjected to an axial compression load for a period of time, additional compressive stress and strain develop in the longitudinal reinforcement due to creep while the stress of concrete decreases. According to McGregor (1997), such redistribution of compressive loads between the concrete and reinforcement can be modeled using an age-adjusted effective modulus E_{caa} (t, t_0) and an age-adjusted transformed area A_{traa} as follows.

$$\varepsilon_{cr}(t, t_0) = \left(\frac{P_{sus}}{A_{traa}}\right)\frac{1}{E_{caa}(t, t_0)} \tag{1}$$

$$E_{caa}(t, t_0) = \frac{E_{ct}(t_0)}{1 + \chi(t_0)[E_{ct}(t_0)/E_{ct}(28)]\phi(t, t_0)} \tag{2}$$

$$A_{traa} = A_c + n_{aa}A_s \tag{3}$$

where ε_{cr} (t, t_0) = creep shortening of reinforced concrete at time t; t_0 = time at loading from concrete placing; E_{ct} (28) = elastic modulus of the concrete at the age of 28 days; $\chi(t_0)$ = aging coefficient addressing the reduction of compression load in the concrete due to creep; $\phi(t, t_0)$ = creep coefficient at time t; A_c and A_s = areas of the concrete and longitudinal reinforcement, respectively; n_{aa} = age-adjusted modular ratio between the reinforcement and concrete (= E_s/E_{caa} (t, t_0)); and E_s = elastic modulus of the reinforcement (= 200 GPa). The aging coefficient $\chi(t_0)$ and creep coefficient $\phi(t, t_0)$ of concrete

are defined as follows [McGregor (McGregor 1997) and ACI 209R-92 (ACI Committee 209 1992)].

$$\chi(t_0) = \frac{t_0^{0.5}}{1 + t_0^{0.5}} \tag{4}$$

$$\phi(t, t_0) = \frac{(t - t_0)^{0.6}}{10 + (t - t_0)^{0.6}} \tag{5}$$

The creep shortening of Eq. (1) can be rewritten as the function of the elastic shortening ε_{a0} at loading age t_0 as follows.

$$\begin{aligned}\varepsilon_{cr}(t, t_0) &= \left(\frac{P_{sus}}{E_{ct}(t_0)A_{tr}}\right)\left(\frac{A_{tr}}{A_{traa}}\right)\left[1 + \chi(t_0)\left[\frac{E_{ct}(t_0)}{E_{ct}(28)}\right]\phi(t, t_0)\right] \\ &= \varepsilon_{a0}\left(\frac{1 + n\bar{\rho}}{1 + n_{aa}\bar{\rho}}\right)\left[1 + \chi(t_0)\left[\frac{E_{ct}(t_0)}{E_{ct}(28)}\right]\phi(t, t_0)\right]\end{aligned} \tag{6}$$

where ε_{a0} = elastic shortening of reinforced concrete at time t_0; A_{tr} = transformed area of the column section at time t_0 ($=A_c + [E_s/E_{ct}(t_0)]A_s$); n = modular ratio between the reinforcement and concrete ($=E_s/E_{ct}(t_0)$); and $\bar{\rho}$ = reinforcement-to-concrete area ratio ($=A_s/A_c$). According to ACI 209R-92 (ACI Committee 209 1992) and Fintel et al. (1987), the elastic modulus $E_{ct}(t_0)$ at time t_0 of normal-weight concrete can be defined as follows.

$$E_{ct}(t_0) = 5000\sqrt{f'_{ct}(t_0)} \tag{7}$$

$$f'_{ct}(t_0) = \left(\frac{t_0}{4.0 + 0.85t_0}\right)f'_{ct}(28) \tag{8}$$

where $E_{ct}(t_0)$ and $f'_{ct}(t_0)$ = time-dependent elastic modulus and compressive strength of concrete, respectively, and $f'_{ct}(28)$ = compressive strength of concrete at the age of 28 days ($=f'_c$).

Since the age-adjusted effective modulus $E_{caa}(t, t_0)$ of Eq. (1) accounts only for the creep effects, the shrinkage shortening needs to be additionally addressed. As shown in Fig. 8b, the shrinkage shortening $\varepsilon_{sh}(t, t_0)$ of reinforced concrete column at time t is smaller than the shrinkage shortening $\varepsilon_{cs}(t, t_0)$ of plain concrete column, because the longitudinal reinforcement restrains shrinkage in concrete. From the force equilibrium, the increase in the compression force of the longitudinal reinforcement due to the shrinkage shortening, $\varepsilon_{sh}(t, t_0)E_sA_s$, should be equal to the decrease in the compression force of the concrete, $[\varepsilon_{cs}(t, t_0) - \varepsilon_{sh}(t, t_0)]E_{caa}(t, t_0)A_c$ (refer to Fig. 8b). Therefore, $\varepsilon_{sh}(t, t_0)$ can be calculated as follows.

$$\varepsilon_{sh}(t, t_0) = \varepsilon_{cs}(t, t_0)\left(\frac{1}{1 + n_{aa}\bar{\rho}}\right) \tag{9}$$

In Eq. (9), the shrinkage shortening $\varepsilon_{cs}(t, t_0)$ of the plain concrete at time t from loading age t_0 can be determined as follows [ACI 209R-92 (ACI Committee 209 1992)].

$$\varepsilon_{cs}(t, t_0) = \varepsilon_{shu}\left[\frac{(t - t_s)}{35 + (t - t_s)} - \frac{(t_0 - t_s)}{35 + (t_0 - t_s)}\right] \tag{10}$$

where t_s = age of the concrete in days when shrinkage begins. t_s, which is earlier than t_0, can be taken as the age of the end of moisture curing.

The total axial shortening $\varepsilon_a(t, t_0)$ of concentrically and eccentrically loaded column is then calculated by adding the creep and shrinkage shortenings in Eqs. (6) and (9).

$$\begin{aligned}\varepsilon_a(t, t_0) &= \varepsilon_{cr}(t, t_0) + \varepsilon_{sh}(t, t_0) \\ &= \varepsilon_{a0}\left(\frac{1 + n\bar{\rho}}{1 + n_{aa}\bar{\rho}}\right)\left[1 + \chi(t_0)\left[\frac{E_{ct}(t_0)}{E_{ct}(28)}\right]\phi(t, t_0)\right] \\ &\quad + \varepsilon_{cs}(t, t_0)\left(\frac{1}{1 + n_{aa}\bar{\rho}}\right)\end{aligned} \tag{11}$$

Figure 9 compares the axial shortenings of the column specimens predicted by Eq. (11) with the test results. The predictions and test results are presented as the circles and solid lines, respectively. The solid lines are the mean of ε_{RC} and ε_{LC} measured at the three heights, 100, 400, and 700 mm (see Figs. 5 and 6). For the predictions, P_{sus} = 421 and 842 kN, A_c = 58,800 mm^2, A_s = 1200 mm^2, and $\bar{\rho}$ = 0.0204 (see Fig. 2b) were applied. For the creep and shrinkage of the concrete increasing with time, t_0 = 37 days, t_s = 7 days, $\chi(t_0)$ = 0.859, f'_c = 47.3 MPa, and n = 5.69 were used. The ultimate creep coefficient ϕ_u and shrinkage strain ε_{shu} of concrete in the column specimens were modified considering the actual loading age and member size as follows. According to ACI 209R-92 (ACI Committee 209 1992), the creep correlation factor for loading age t_{LA} was taken as $\gamma_{LA} = 1.25(t_{LA})^{-0.118} = 0.816$ by using $t_{LA} = t_0 = 37$ days. The creep and shrinkage correlation factors for member size (i.e. the volume-to-surface ratio VS = 60 mm) were taken as $\gamma_{VS} = 2/3[1 + 1.13\exp(-0.0213\,VS)] = 0.877$ and $1.2\exp(-0.00472VS)] = 0.904$, respectively.

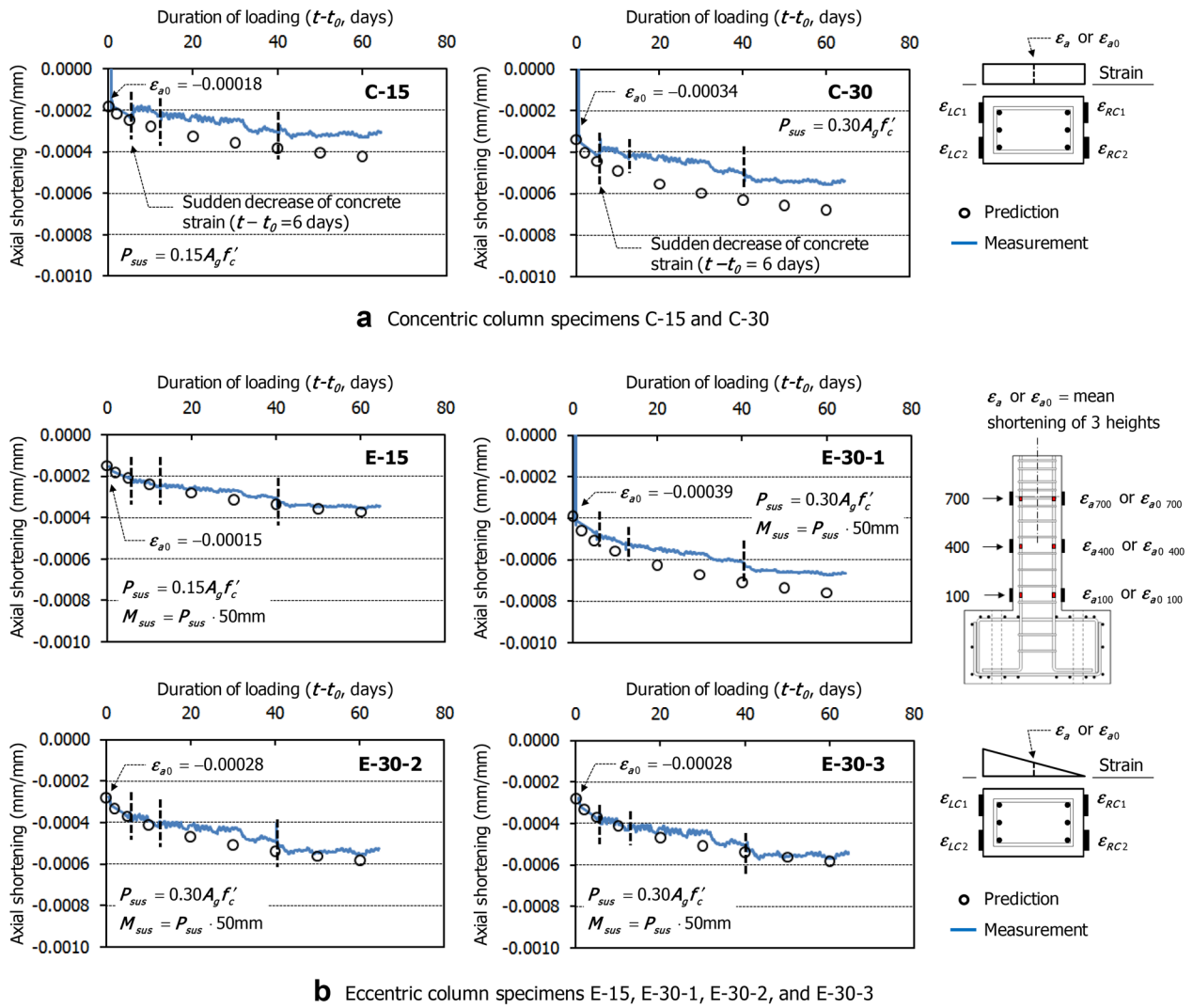

Fig. 9 Comparisons of predicted and measured axial shortenings of concentrically and eccentrically loaded column specimens.

Therefore, the ultimate creep coefficient and shrinkage strain for the column specimens were determined as $\phi_u = \gamma_{LA}\gamma_{VS}\phi'_u = 0.816 \cdot 0.877 \cdot 2.25 = 1.61$ and $\varepsilon_{shu} = \gamma_{VS}\varepsilon'_{shu} = 0.904 \cdot 0.000672 = 0.000607$. Since the sustained load tests of the column specimens were started at time $t_0 = 37$ days, the effects of the creep and shrinkage of concrete on the axial shortenings of the column specimens were predicted between $t = 37$ days and 101 days (duration = 64 days). The time-dependent creep coefficient $\phi(t, t_0)$ and shrinkage strain $\varepsilon_{cs}(t, t_0)$ increasing with time were calculated by Eqs. (5) and (10), respectively. Note that the elastic shortening ε_{a0} of each column specimen was used as the values measured by the strain gages so that uncertainty in the prediction of elastic shortening could not influence the prediction of long-term axial shortening. The elastic shortenings ε_{a0} of the column specimens are presented in Fig. 9.

As shown in Fig. 9a, the predicted axial shortenings of concentrically loaded column specimens C-15 and C-30 were greater that the measured shortenings. The low temperature of laboratory might affect discrepancies between the measured and predicted results. If the unexpected increase in the measured axial shortenings that occurred during the re-tightening process of post-tensioning rods were taken into account (particularly at $t - t_0 = 43$ days), the correlations between the predictions and measurements were reasonable. Figure 9(b) compares the predicted and measured axial shortenings of eccentrically loaded column specimens E-15, E-30-1,

E-30-2, and E-30-3. Despite non-uniform strain distributions, Eq. (11) based on the hypothesis of uniform strain distribution over the section predicted well the axial shortenings increasing with time.

4.2 Curvature (or Lateral Displacement)

For eccentrically loaded columns, the time-dependent creep curvature $\kappa_{cr}(t, t_0)$ of the uncracked section can be defined based on the age-adjusted effective modulus E_{caa} (t, t_0) and an age-adjusted transformed moment of inertia I_{traa} as follows (see Fig. 10a).

$$\kappa_{cr}(t,t_0) = \left(\frac{M_{sus}}{I_{traa}}\right)\frac{1}{E_{caa}(t,t_0)} = \left(\frac{M_{sus}}{E_{ct}(t_0)I_{traa}}\right)\left[1+\chi(t_0)\left[\frac{E_{ct}(t_0)}{E_{ct}(28)}\right]\phi(t,t_0)\right] \tag{12}$$

$$I_{traa} = I_c + n_{aa}I_s \tag{13}$$

where M_{sus} = sustained bending moment and I_c and I_s = moments of inertia of the concrete and reinforcement calculated about the geometrical center of the section. Figure 10 illustrates I_c and I_s of a rectangular section with asymmetric reinforcement arrangement. The creep curvature κ_{cr} (t, t_0) in Eqs. (12) and (13) are formulated similar to the creep shortening ε_{cr} (t, t_0) in Eqs. (1) to (3), based on the linear elastic behavior and reduced elastic modulus E_{caa} (t, t_0) of the concrete. By replacing ε_{cr} (t, t_0) and ε_{c0} in Eq. (6) with κ_{cr} (t, t_0) and κ_0, respectively, the creep curvature κ_{cr} (t, t_0) can be defined as the function of the elastic curvature κ_0 at time t_0.

$$\begin{aligned}\kappa_{cr}(t,t_0) &= \left(\frac{M_{sus}}{E_{ct}(t_0)I_{tr}}\right)\left(\frac{I_{tr}}{I_{traa}}\right)\left[1+\chi(t_0)\left[\frac{E_{ct}(t_0)}{E_{ct}(28)}\right]\phi(t,t_0)\right]\\ &= \kappa_0\left(\frac{1+n\bar{\eta}}{1+n_{aa}\bar{\eta}}\right)\left[1+\chi(t_0)\left[\frac{E_{ct}(t_0)}{E_{ct}(28)}\right]\phi(t,t_0)\right]\end{aligned} \tag{14}$$

where I_{tr} = transformed moment of inertia $(=I_c+[E_s / E_{ct}(t_0)]\, I_s)$ and $\bar{\eta}$ = ratio between moments of inertia of reinforcing steel bars and concrete $(=I_s/I_c)$. Equation (14) represents the curvature increasing with time by the creep of concrete.According to Park and Paulay (1975), shrinkage can also cause a long-term curvature increasing over time particularly in unsymmetrically reinforced columns. Figure 10b illustrates the long-term curvature κ_{sh} (t, t_0) caused by the shrinkage of concrete. For formulation, it is assumed that the column has different reinforcement areas A_{st} and A_{sb} at both ends and A_{st} is greater than A_{sb} (see Fig. 10a). Due to the unequal restraints of A_{st} and A_{sb} against the shrinkage of concrete, a shrinkage curvature κ_{sh} (t, t_0) as well as the shrinkage shortening ε_{sh} (t, t_0) increasing with time occur (see Fig. 10b). Since there is no gain or loss of moment at the section after the concrete shrinkage, the moment created by the concrete should be cancelled out that by the unequal reinforcements A_{st} and A_{sb}. Thus,

$$\begin{aligned}E_{caa}I_c\kappa_{sh}(t,t_0) = {} & E_s[\varepsilon_{sh}(t,t_0) - \kappa_{sh}(t,t_0)\cdot y_t]A_{st}y_t\\ & - E_s[\varepsilon_{sh}(t,t_0) + \kappa_{sh}(t,t_0)\cdot y_b]A_{sb}y_b\end{aligned} \tag{15}$$

where y_b and y_t = distances of the reinforcements A_{sb} and A_{st} from the geometrical center of the section. In Eq. (15), the shrinkage shortening ε_{sh} (t, t_0) is calculated from Eq. (9). By using $I_s \approx A_{st}y_t^2 + A_{sb}y_b^2$, $n_{aa} = E_s/E_{caa}$, and $\bar{\eta} = I_s/I_c$, Eq. (15) can be rewritten as follows.

$$\kappa_{sh}(t,t_0) = \varepsilon_{sh}(t,t_0)\left(\frac{A_{st}y_t - A_{sb}y_b}{I_c}\right)\left(\frac{n_{aa}}{1+n_{aa}\bar{\eta}}\right) \tag{16}$$

The total time-dependent curvature κ (t, t_0) of eccentrically loaded column can be calculated by adding or

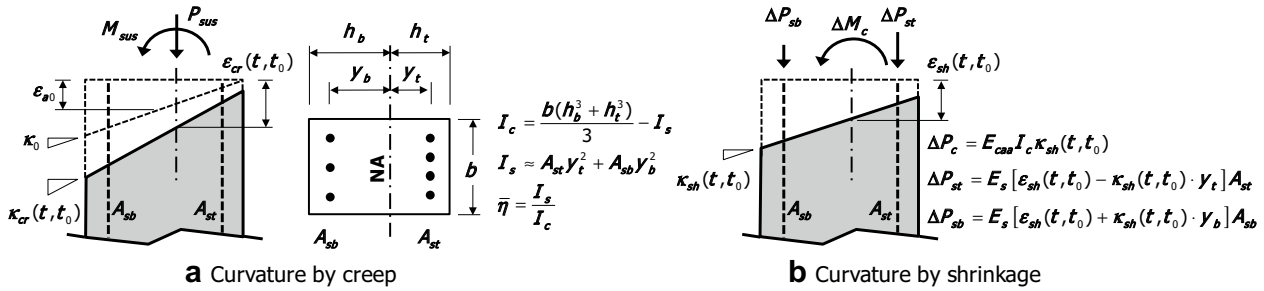

Fig. 10 Time-dependent curvature of eccentrically loaded column specimens.

subtracting the shrinkage curvature $\varepsilon_{sh}(t, t_0)$ to the creep curvature $\varepsilon_{cr}(t, t_0)$.

$$\kappa(t,t_0) = \kappa_{cr}(t,t_0) \pm \kappa_{sh}(t,t_0) = \kappa_0\left(\frac{1+n\bar{\eta}}{1+n_{aa}\bar{\eta}}\right)\left[1+\chi(t_0)\left[\frac{E_{ct}(t_0)}{E_{ct}(28)}\right]\phi(t,t_0)\right] \pm \varepsilon_{sh}(t,t_0)\left(\frac{A_{st}y_t - A_{sb}y_b}{I_c}\right)\left(\frac{n_{aa}}{1+n_{aa}\bar{\eta}}\right) \quad (17)$$

In Eq. (17), the minus sign is used when the areas of the reinforcements are reversed (i.e. $A_{sb} > A_{st}$). Note that the shrinkage curvature $\kappa_{sh}(t, t_0)$ of Eq. (17) is vanished in symmetrically reinforced sections because $A_{sb}=A_{st}$ and $y_b=y_t$.The long-term curvatures of eccentrically loaded column specimens E-15, E-30-1, E-30-2, and E-30-3 were evaluated using Eq. (17). Since the column specimens were symmetrically reinforced, the effect of the shrinkage on the curvature was ignored: $\kappa_{sh}(t, t_0)=0$. Furthermore, since the column specimens were subjected to uniform moment M_{sus}, the immediate curvature κ_0 and long-term curvature $\kappa(t, t_0)$ of Eq. (17) can be replaced with the lateral displacements δ_0 and $\delta(t, t_0)$ at the top, respectively.

$$\delta(t,t_0) = \delta_0\left(\frac{1+n\bar{\eta}}{1+n_{aa}\bar{\eta}}\right)\left[1+\chi(t_0)\left[\frac{E_{ct}(t_0)}{E_{ct}(28)}\right]\phi(t,t_0)\right] \quad (18)$$

where δ_0=elastic lateral displacement at time t_0 and $\delta(t, t_0)$=long-term lateral displacement at time t.

Figure 11 compares the predicted and measured lateral displacements $\delta(t, t_0)$ increasing with time. The predicted and measured are presented with the circles and solid lines, respectively. For the prediction of $\delta(t, t_0)$, $\phi_u=1.61$, $\varepsilon_{shu}=0.000607$, $t_0=37$ days, $t=37$–101 days, $\chi(t_0)=0.859$, $n=5.69$, $I_c=4.37\cdot10^8$ mm^4, $I_s=1.26\cdot10^7$ mm^4, and $\bar{\eta}=0.0287$ were used. The creep coefficient $\phi(t, t_0)$ was calculated by Eq. (5). The elastic lateral displacement δ_0 of each column specimen was used as the values measured by the LVDTs, shown in Fig. 11. The lateral displacements measured by the LVDTs were disturbed at $(t-t_0)=42$, 50, and 78 days during the re-tightening process of post-tensioning rods. If such measurement errors were taken into account, the agreements between the predicted and measured lateral displacements might be better.

The lateral displacement at the top of the eccentrically loaded column specimens can also increase due to the second-order effect (i.e. *P-Δ* effect). However, the specimens were the short columns where the slenderness effect can be neglected [ACI 318 (ACI Committee 318 2014)].

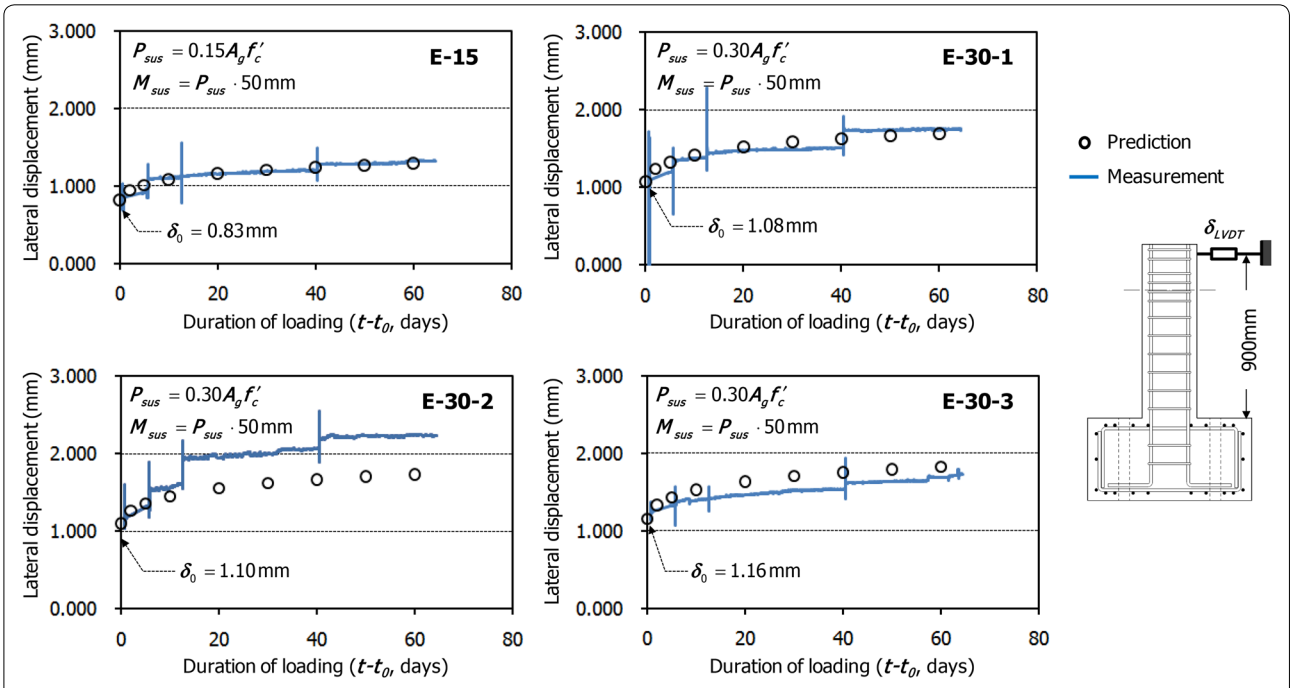

Fig. 11 Comparisons of predicted and measured lateral displacements of eccentrically loaded column specimens.

5 Summary and Conclusions

For eccentrically loaded columns subjected to combined moment and axial load, curvature (or lateral displacement) and axial shortening increase with time due to the creep and shrinkage of concrete. In this study, the time-dependent deformations in eccentrically loaded column were investigated. Six cantilever column specimens were concentrically or eccentrically loaded for 64 days and the long-term deformations depending on the magnitude of axial load and eccentricity were investigated. Such long-term deformations were predicted based on the age-adjusted effective modulus of concrete and transformed section properties. The results of the present study were summarized as follows.

1) For the eccentrically loaded column specimens, the lateral displacement due to eccentric moment and axial shortening due to axial compression increased with time. The increasing rates of such long-term deformations rapidly decreased with increasing time.
2) The axial shortenings of eccentrically loaded columns were the almost same as that of the concentrically loaded column. The axial shortenings of the eccentrically and concentrically loaded columns agreed well with the predictions based on the existing creep and shrinkage models of concrete specified in ACI 209R-92.
3) The curvature or lateral displacement of the eccentrically loaded columns, increasing with time, were also predicted based on the age-adjusted effective modulus of concrete and the concrete creep and shrinkage models in ACI 209R-92. The predicted long-term lateral displacements agreed reasonably with the test results.

As investigated in this study, the sustained moment and resulting long-term deformation increases differential shortening between compression members under construction and ultimately changes member forces by redistributing loads. Thus when designing compression members subjected to high axial load, the effects of the sustained moment and long-term deformation on the behavior of the compression members should be considered.

Authors' Contributions

TSE: Planning and Performing Experiments, Analyzing Experimental Results, and Drafting the Manuscript. CSK, XZ: Analyzing Experimental Results, and Revising the Manuscript. JYK: Performing Experiments, Analyzing Experimental Results, and Revising the Manuscript. All authors read and approved the final manuscript.

Author details

[1] Dept. of Architectural Engineering, Dankook University, 152 Jukjeon-ro, Suji-gu, Yongin-Si, Gyeonggi-do 16890, South Korea. [2] School of Civil Engineering at Shandong Jianzhu Univ. and Shandong Provincial Key Lab. of Appraisal and Retrofitting in Building Structures, Jinan, Shandong 250101, People's Republic of China. [3] Dept. of Architectural Engineering, Kwangwoon University, 20 Kwangwoon-ro, Nowon-Gu, Seoul 01897, South Korea.

Acknowledgements

This research was supported by a grant (Code No. 18CTAP-C129746-02, Land & Transport Technology Promotion Research Program) funded by the Ministry of Land, Infrastructure and Transport of Korea.

Competing Interests

The authors declare that they have no competing interests.

Availability of Data and Materials

The datasets used during the current study are available from the corresponding author on reasonable request.

Funding

All experiment were financially supported by the Korea Agency for Infrastructure Technology Advancement (KAIA) funded by the Ministry of Land, Infrastructure and Transport (Grant No. 18CTAP-C129746-02).

Publisher's Note

Received: 3 July 2018 Accepted: 4 October 2018
Published online: 29 December 2018

References

ACI Committee 209. (1992). *Prediction of creep, shrinkage and temperature effects in concrete structures, ACI 209R-92* (p. 47). Farmington Hills: American Concrete Institute.

ACI Committee 318. (2014). *Building code requirements for structural concrete and commentary, ACI 318-14*. Farmington Hills: American Concrete Institute.

Balaguru, P., & Nawy, E. G. (1982) *Evaluation of creep strains and stress redistribution in RC columns*. ACI Special Publication, SP76-12, pp. 309–324.

Bradford, M. A. (1997). Service load analysis of slender reinforced concrete columns. *ACI Structural Journal, 94*(6), 675–683.

European Committee for Standardization. (2004). *Eurocode 2: Design of concrete structures—Part 1-1: General rules and rules for buildings, BS EN 1992-1-1: 2004* (p. 2004). London: British Standards Institute.

Fintel, M., Ghosh, S. K., & Iyengar, H. (1987). *Column shortening in tall structure—prediction and compensation, EB108.01D* (p. 35). Skokie: Portland Cement Association.

Green, R., & Breen, J. E. (1969). Eccentrically loaded concrete columns under sustained load. *Proceedings of ACI Journal, 66*(11), 866–874.

Kim, J. Y., & Abdelrazaq, A. K. (2009). Construction sequence analysis of the flat plate system in a high-rise building and its impact on the construction cycle. *The Structural Design of Tall and Special Buildings, 18*(3), 341–349.

Korean Concrete Institute (KCI). (2012). *Design code for structural concrete, KCI 2012*. Seoul: Korean Concrete Institute.

Maru, S., Asfaw, M., Sharma, R. K., & Nagpal, A. K. (2003). Effect of creep and shrinkage on RC frames with high beam stiffness. *Journal of Structural Engineering, ASCE, 129*(4), 536–543.

McGregor, J. G. (1997). *Reinforced concrete: Mechanics and design* (3rd ed., p. 938). New Jersey: Prentice Hall Inc.

Mickleborough, N. C., & Gilbert, R. I. (1991) *Creep Buckling of uniaxially loaded reinforced concrete columns*. ACI Special Publication, SP129-03, pp. 39–53.

Park, R., & Paulay, T. (1975). *Reinforced concrete structures* (p. 769). New York: Wiley.

Tatsa, E. Z. (1989). Load carrying of eccentrically loaded reinforced concrete panels under sustained load. *ACI Structural Journal, 86*(2), 150–155.

Viest, I. M., Elstner, R. C., & Hognestad, E. (1955). Sustained load strength of eccentrically loaded short reinforced concrete columns. *Journal of the American Concrete Institute, 27*(7), 727–755.